Persulfate Activation by Ferrocene-based Metal-organic Framework Microspheres for Efficient Oxidation of Organic Pollutants

Xiaoyu Lv
University of Jinan
Yanqiu Leng
Shandong Academy of Environmental Science
Rongyao Wang
University of Jinan
Yan Wei
University of Jinan
Xiaohua Ren
University of Jinan
Weilin Guo (chm_guowl@ujn.edu.cn)
University of Jinan https://orcid.org/0000-0002-5684-8954

Research Article

Keywords: Metal-organic frameworks, persulfate, sulfate radical, acid orange 7, catalytic degradation, transition metal

Posted Date: October 15th, 2021

DOI: https://doi.org/10.21203/rs.3.rs-813604/v1

Abstract

Ferrocene-based metal-organic framework with different transition metals (M-Fc-MOFs, M=Fe, Mn, Co) were synthesized by a simple hydrothermal method and used as a heterogeneous catalyst for persulfate activation. The samples were characterized by X-ray diffraction, transmission electron microscopy, X-ray electron spectroscopy, cyclic voltammetry and electrochemical impedance spectroscopy. Meanwhile, the influences of factors such as catalyst dosage, persulfate concentration and pH on the degradation of acid orange 7 (AO7) were studied in detail. The results showed that hollow cobalt-based ferrocenyl metal-organic framework microspheres (Co-Fc-MOFs) exhibited the best catalytic performance, which is closely related to the synergy of Fc/Fc^{+} and Co^{2+}/Co^{3+} cycles in persulfate activation. Free radical quenching studies indicated that both sulfate and hydroxyl appeared to contribute to the degradation of AO7.

1. Introduction

In recent years, water pollution caused by excessive use and excessive discharge of dyes has posed a serious threat to the world (Mu et al. 2019; Marković et al. 2019). A large amount of dye wastewater is directly discharged into the water environment and soil without treatment (Khatri et al. 2015). Therefore, the development of economical and environmentally friendly water treatment technology to remove organic dyes has become a top priority.

Advanced oxidation processes (AOPs) based on persulfate (PS) activation are considered to be one of the most promising strategies to effectively remove organic pollutants in sewage. For the past few years, AOPs have been applied to eliminate acid orange 7 (AO7) by several researchers. It has gained tremendous importance due to the high stability and moderate cost of PS (Wacławek et al. 2017). There are numerous approaches to activate PS. Compared with these energy-based methods (such as UV light, microwave and heat), transition metal activation is generally more readily to conduct and more cost-effective, thereby having been frequently chosen as the activators for PS (Li et al. 2015; Usman et al. 2012; Stroever et al. 2015).

Metal-organic frameworks (MOFs) are a porous coordination polymer composed of metal ions and organic linkers (Devic et al. 2005; Li, Yang, and Colloids 2007; He et al. 2014). In addition, compared with the traditional activated persulfate catalyst, MOFs catalysts have the characteristics of large specific surface area, high porosity, adjustable porosity, good thermal stability and abundant active sites (Eddaoudi et al. 2002; Liu et al. 2007; Xiong et al. 2015; Yang et al. 2017; Chang et al. 2019). Gao et al. investigated the catalytic performance of MIL-53 as heterogeneous catalysts of PS, their results demonstrated that the accelerated catalytic degradation of organic pollutants was obtained in the presence of PS (Gao et al. 2017). Li et al. prepared Cu@Co-MOFs composite material that has excellent catalytic performance for methylene blue (MB) removal from water, which makes it an ideal candidate for heterogeneous catalysis (Li et al. 2019). Ferrocene-based metal-organic framework with different transition metals (M-Fc-MOFs, M = Fe, Mn, Co) prepared by Huo et al. have hydrogen storage properties

and magnetic properties, but their catalytic properties are rarely studied (Huo et al. 2012). Therefore, we carried out a study on M-Fc-MOFs activated persulfate degradation of organic pollutants.

In this work, Fe-Fc-MOFs. Mn-Fc-MOFs and Co-Fc-MOFs were synthesized by hydrothermal method, and their physical and chemical properties were characterized. In addition, we evaluated the ability of Co-Fc-MOFs activated persulfate to degrade AO7. The effects of persulfate dosage, catalyst dosage and pH, as well as the stability of the catalyst were investigated. The possible reaction mechanism of persulfate activation was discussed.

2. Materials And Methods

2.1. Chemicals

All chemicals were used directly as obtained with no further purification in this study. N,N'-dimethylformamide (DMF), 1,1'-ferrocenedicarboxylic acid ($Fc(COOH)_2$, > 97% (HPLC)), ferric chloride hexahydrate ($FeCl_3 \cdot 6H_2O$), manganese chloride hexahydrate ($MnCl_2 \cdot 6H_2O$), cobalt chloride hexahydrate ($CoCl_2 \cdot 6H_2O$) and potassium PS ($K_2S_2O_8$) were purchased from Shanghai Macklin Co., Ltd. (Shanghai, China).

2.2. Preparation of catalyst

The typical method to prepare the ferrocenyl metal-organic framework microspheres is as follow: a mixture of 0.16 g (0.6 mmol) $FeCl_3 \cdot 6H_2O$ in 6 mL DMF and 0.16 g (0.6 mmol) $Fc(COOH)_2$ in 6 mL DMF was added into a 100 mL poly tetra fluoroethylene (PTFE) bottle and sealed in a stainless steel autoclave. The sealed pressure bomb is slowly heated (2°C/min) in an oven, heated from room temperature to 125°C, kept at this temperature for 10 h, and then cooled to room temperature. The precipitate was collected by centrifugation, washed with DMF and then repeatedly washed with ethanol until the upper solution was clear. The samples were vacuum dried at 70°C for 24 hours to obtain Fe-Fc-MOFs. Mn-Fc-MOFs and Co-Fc-MOFs were prepared according to the same synthetic methods (Huo et al. 2012).

2.3 Degradation experiments

The catalytic performances of Fe-Fc-MOFs, Mn-Fc-MOFs and Co-Fc-MOFs were evaluated by the removal of AO7 in aqueous solution. At ambient temperature, adsorption and degradation tests were performed in a typical batch mode by using three flasks (50 mL). Fe-Fc-MOFs, Mn-Fc-MOFs and Co-Fc-MOFs (5 mg) were dispersed into AO7 solution (20 mL, 20 mg/L), and the mixture was stirred for 60 min to establish an adsorption/desorption equilibrium. PS (1.6 mL, 50 mmol/L) was then added to the mixed solution. At a certain time interval, take a small amount of the mixture and centrifuge at a speed of 6000 rpm for a short time for 3 minutes to remove the solid catalyst. Measure the residual concentration of AO7 with an ultraviolet spectrophotometer, and the analysis wavelength is 484nm.

2.4 Characterization and analysis methods

The XRD patterns of the as-prepared products were obtained using a RigakuDmax/Ultima IV diffractometer in the range of 2θ = 2°-60° with Cu Kα radiation. The morphological analysis was performed by scanning electronic microscopy (SEM, S4800, Hitachi Corporation, Germany). FTIR spectra were performed by KBr pellets on Nicolet 6700 spectrometer in the range of 4,000–450 cm-1 at indoor temperature. The chemical states of samples were studied by XPS, and the XPS spectra were recorded with a Surface Science Instrument SSX-100. CV and EIS were performed by the CHI608C electrochemical analyzer with samples as the working electrode.

3. Results And Discussion

3.1 Morphology and textural characteristics

In this study, ferrocene-based metal-organic framework were synthesized by the solvothermal reaction of Fe^{3+}, Mn^{2+}, Co^{2+} with 1,1'-ferrocenedicarboxylic acid in DMF. By connecting metal ions with this multidentate organic ligand, three different metal-organic framework microspheres referred as Fe-Fc-MOFs, Mn-Fc-MOFs, Co-Fc-MOFs were prepared under similar conditions. The precipitates were isolated and collected by centrifugation and then washed several times with DMF and ethanol. The reaction temperature, reaction time, and molar ratio of reactants play critical roles in the formation of spherical particles.

The XRD patterns of Fe-Fc-MOFs, Mn-Fc-MOFs and Co-Fc-MOFs were shown in Fig. 1. The XRD results indicated that the Fe-Fc-MOFs, Mn-Fc-MOFs and Co-Fc-MOFs were isostructural to the previous report (Huo et al. 2010). Obviously, the distinct peaks at 2θ of 6.24, 12.52, 14.68, 16.44 and 18.84 indicated the high crystallinity of Fe-Fc-MOFs. The diffraction patterns of Fe-Fc-MOFs, Mn-Fc-MOFs and Co-Fc-MOFs share feature peaks, thus showing that the three-prepared samples contain part of similar structural information. In addition, the sharp features of these peaks also indicate that the local crystalline is of high ordering and of small size. Despite of the existence of some peaks in almost the same position in the XRD patterns, each of the three patterns of Fe-Fc-MOFs, Mn-Fc-MOFs and Co-Fc-MOFs includes small part of particular peaks that feature their uniqueness, which may be due to the differences in the structure of a single phase, or the existence of several distinct phases.

The SEM images (Fig. 2a–i) show that the samples have a spherical shape with an average diameter around 8 ~ 20 μm. Higher magnification SEM images (Fig. 2b, e and i) indicate that the spherical particles are composed of nanosheets instead of smooth-like spherical colloids, which are possibly caused by the layered structure of Co-Fc-MOFs. Obviously, these three catalysts have the same structure (Huo et al. 2010).

FT-IR verified the formation of metal-organic framework. The FT-IR spectra of Co-Fc-MOFs and $Fc(COOH)_2$ further confirmed that cobalt ions and dicarboxylic acid functionalized organometallic ligands formed metal-organic framework, as evidenced by a red shift of CO stretching frequency from 1687 cm^{-1} for the organometallic precursor to 1581.7 cm^{-1} for the metal-organic framework (Fig. 3) (Su et al. 2013). FT-IR

result was consistent with the crystal structures of XRD and other similar carboxylic acid metal-organic framework (Huo et al. 2010).

3.2 A adsorption and catalytic performance of catalyst

The catalytic performance of as-synthesized Fe-Fc-MOFs, Mn-Fc-MOFs and Co-Fc-MOFs had been assessed for degradation of AO7 with the presence of PS. Figure 4 displays the AO7 degradation efficiency under various reaction systems. As expected, the presence of catalyst significantly enhanced AO7 removal. Minimum degradation of AO7 (7.69%) was obtained with PS alone, showing that PS can induce AO7 degradation. Co-Fc-MOFs exhibited the highest degradation rate, and an approximate 83.7% of AO7 was removed from the solution after 90 min. AO7 removal on Mn-Fc-MOFs was 16.35% lower than on Co-Fc-MOFs. Fe-Fc-MOFs also showed good catalytic activity and the degradation rate of AO7 was 54.55% within 90 min. The results showed that the presence of Co ions significantly improved the catalytic activity of the catalyst. Because iron, cobalt and manganese have a variable valence state, that is to say, all of them can produce redox reaction to promote the decomposition of PS. In order to achieve the best experimental results, the Co-Fc-MOFs catalyst was used in subsequent experiments.

Figure 5a presented the degradation of AO7 under different persulfate concentrations when the fixed concentration of Co-Fc-MOFs is 200 mg/L. The degradation rate of AO7 increased from 73–89% with increasing persulfate concentration from 2 to 8 mmol/L within 120 min in Co-Fc-MOFs/PS system. It showed that too high persulfate concentration can promote the degradation of AO7, which were probably the result of increased generation of •OH and $SO_4^{\bullet-}$ radicals. Nevertheless, further addition of PS, i.e.15 mmol/L, may lead to reduction of degradation efficiency of AO7, mainly due to the excess of PS generating sulfate anions. In addition, $SO_4^{\bullet-}$ could be oxidized by $S_2O_8^{2-}$(Eqs. (1) and (2)).

$$SO_4^{\bullet-} + SO_4^{\bullet-} \rightarrow S_2O_8^{2-} \quad (1)$$

$$SO_4^{\bullet-} + S_2O_8^{2-} \rightarrow S_2O_8^{-\bullet} + SO_4^{2-} \quad (2)$$

As shown in Fig. 5b, AO7 degradation efficiency was about 8% without catalysts in 120 min. After adding 100 mg/L Co-Fc-MOFs, the degradation efficiency increased to 67%. The phenomena indicated that Co-Fc-MOFs could effectively catalyze the decomposition and degradation of AO7 by persulfate. When the dosage of Co-Fc-MOFs is increased to 200 mg/L, the removal rate of AO7 is about 82%. It was explained that increasing the Co-Fc-MOFs dosage could directly enhance absorption in this system. When the dosage of Co-Fc-MOFs was increased from 300 mg/L to 500 mg/L, the degradation efficiency did not change significantly. The possible reason for this phenomenon was that the absorption effect on Co-Fc-MOFs for 4 mmol/L persulfate activation was attained at an equilibrium level when the concentration of Co-Fc-MOFs was 300 mg/L. This result indicates that the catalyst has a perfect catalytic effect on activating PS to generate free radicals. Increasing the amount of catalyst indicates that the generation of active centers and Co^{2+} ions in the PS solution increases, which will generate more free radicals. The

catalyst released by Co in the active center and cobalt ions enhances more free radicals through the oxidation of PS.

The pH value of the solution has a significant impact on the performance of various redox systems. Figure 5c showed the effect of solution pH on the catalytic oxidation of AO7. With the increase of pH value, the degradation rate of AO7 also increased, indicating that Co-Fc-MOFs can improve the degradation rate of AO7 under alkaline conditions. Because Co^{2+} on the surface of Co-Fc-MOFs reacts with H_2O to form $CoOH^+$ (Eqs. (3)). $CoOH^+$ activates PS to produce $SO_4^{\bullet-}$ (Eqs. (4)) (Su et al. 2013). $SO_4^{\bullet-}$ has a high oxidation-reduction potential and can effectively oxidize AO7. Under alkaline conditions, $SO_4^{\bullet-}$ can be converted into surface-bound hydroxyl radicals (•OH) (Eqs. (5)) (Liang, Su, and Research 2009). Under acidic conditions, the generation of $CoOH^+$ is limited (Ahmadi et al. 2017). In addition, excess hydrogen ions can scavenge sulfate radicals and hydroxyl radicals, which will adversely affect catalysis (Eqs. (6)). Strong acid conditions inhibit the activation of persulfate, and persulfate is catalyzed by acid (Eqs. (7) and (8)). Therefore, alkaline conditions are conducive to the degradation of AO7.

$Co^{2+} + H_2O \rightarrow CoOH^+$ (3)

$CoOH^+ + S_2O_8^{2-} \rightarrow CoOH^{2+} + SO_4^{2-} + SO_4^{\bullet-}$ (4)

$SO_4^{\bullet-} + OH^- + H^+ \rightarrow \bullet OH + SO_4^{2-} + H^+$ (5)

$SO_4^{\bullet-}/\bullet OH + H^+ + e^- \rightarrow HSO_4^-\bullet / H_2O$ (6)

$H^+ + S_2O_8^{2-} \rightarrow HS_2O_8^-$ (7)

$HS_2O_8^- + H_2O \rightarrow H_2SO_5 + HSO_4^-$ (8)

3.3 Mechanism of persulfate activation

In order to check whether $SO_4^{\bullet-}$ or •OH dominates the degradation of AO7, some alcohols were added to the solutions under study. In this case, tert-butanol (TBA) and ethanol were used based on the differences between the reaction rates of these two radical scavengers with $SO_4^{\bullet-}$ and •OH, respectively. Ethanol is suitable for removing $SO_4^{\bullet-}$ and •OH because of its high reaction rates (the reaction rates of $SO_4^{\bullet-}$ and •OH are $1.6–7.7 \times 10^7\ M^{-1}s^{-1}$ and $1.2–2.8 \times 10^9\ M^{-1}s^{-1}$, respectively (Ghanbari and Moradi 2017)). TBA has a higher scavenging affinity for •OH than $SO_4^{\bullet-}$ (•OH has a reaction rate of $3.8–7.6 \times 10^8\ M^{-1}s^{-1}$, and $SO_4^{\bullet-}$ has a reaction rate of $4.0–9.1 \times 10^5\ M^{-1}s^{-1}$, which is almost 1000 times smaller than that observed with the case of •OH) (Ghanbari and Moradi 2017; Liang, Su, and Research 2009). Therefore, the difference in the degradation yield of AO7 with the participation of ethanol and TBA represents the performance of sulfate radicals (Huo et al. 2010). In the current work, 500 mg/L ethanol was poured into the AO7 solutions, and the AO7 removal rate only reached 22% after 60 min. At the same time, in the case

of 500 mg/L TBA, the removal efficiency was almost 2.5 times that of ethanol, reaching 54% (Fig. 6). Therefore, it can be concluded that the $SO_4^{\bullet-}$ and •OH released by the Co-Fc-MOFs/PS system were the main oxidizing substances that degrade AO7 in the solutions (Ghanbari and Moradi 2017).

Ferrocene and its derivatives are known for their redox properties. Therefore, we used cyclic voltammetry (CV) to study the redox properties of Fe-Fc-MOFs, Mn-Fc-MOFs and Co-Fc-MOFs. The electron transfer ability of the conductive surface of the materials has a great influence on the electrons transfer efficiency between the organic compound and the catalyst. As seen in Fig. 7, the CV curves showed that the higher current density and greater reductive capability of Co-Fc-MOFs to coordinate a redox process than those of Mn-Fc-MOFs and Fe-Fc-MOFs. This result suggested that the electro catalytic activity of Co-Fc-MOFs was superior to that of Mn-Fc-MOFs and Fe-Fc-MOFs. Due to the rapid valence transfer of Fe/Co in the Co-Fc-MOFs composite material, it is conducive to the activation of PS (Liu et al. 2020).

The electrode kinetics and interface reactions to these three catalysts can be further studied by EIS (Duan et al. 2019). It can be clearly seen from Fig. 8, compared with Co-Fc-MOFs, the semicircle diameter of Mn-Fc-MOFs and Fe-Fc-MOFs samples is significantly reduced. It can show that the cobalt ion in the catalyst can significantly reduce the charge transfer resistance compared with the iron ion and the manganese ion, thereby promoting the oxidation-reduction reaction. Hence, the charge separation of the Co-Fc-MOFs was much easier than the Mn-Fc-MOFs and Fe-Fc-MOFs, which corresponded to the experimental result of CV. This result revealed that the cobalt ions could accelerate the processes of electron transfer.

XPS characterization was used to study the chemical state and atomic composition of elements on the catalyst. Figure 9a showed the XPS spectra before and after the Co-Fc-MOFs reaction. From the wide-scan XPS spectrum of Co-Fc-MOFs, the binding energies were 285, 533, 712 and 781 eV, respectively, indicating that C, O, Fe and Co coexist in the sample. It can be noticed that the XPS spectrum of the used Co-Fc-MOFs was almost the same as that of the fresh one, indicating that the catalyst was stable. As we all know, the generation of $SO_4^{\bullet-}$ and •OH is the induction of the electron exchange between Co^{2+}/Co^{3+} and PS in the reaction. The chemical state change of cobalt in fresh and used Co-Fc-MOFs has also been studied. The Co 2p XPS spectrum was shown in Fig. 9b, the photoemission peak centered at 778.1 eV indicates metallic Co. The peaks at 786 and 802.8 eV were typical satellite characteristics of Co^{2+}. The two peaks of Co 2p3/2 and Co 2p1/2 were located at 779.9 and 795.9 eV, respectively, which were displayed in the spectrum, indicating the presence of Co^{3+} in Co-Fc-MOFs (Liu et al. 2016). During the activations of PS, the catalytic activity of Co is higher than that of Fe and Mn.

According to the experimental results, the degradation mechanism of AO7 in Co-Fc-MOFs/PS system was shown in Fig. 10. The interaction between the persulfate of Co-Fc-MOFs and the active site of cobalt can be explained by Eqs. (9) and (10). Ferrocene is produced through self-oxidation and reduction $SO_4^{\bullet-}$ (Eqs. (11) and (12)) (Erdem and Erdem 2020). In the reaction solution, the leaching iron of the Co-Fc-MOFs catalyst can also activate the PS with a chain reaction, thereby generating free sulfate radicals ($SO_{4\ free}^{\bullet-}$) to degrade AO7 (Eqs. (13), (14) and (15)).

$Co^{2+} + S_2O_8^{2-} \rightarrow Co^{3+} + SO_4^{\bullet-} + SO_4^{2-}$ (9)

$S_2O_8^{2-} + H_2O \rightarrow HSO_5^{-} + HSO_4^{-}$ (10)

$Fc + S_2O_8^{2-} \rightarrow Fc^{+} + SO_4^{\bullet-} + SO_4^{2-}$ (11)

$Fc^{+} + S_2O_8^{2-} \rightarrow Fc + S_2O_8^{-\bullet}$ (12)

$Fe^{3+} + S_2O_8^{2-} \rightarrow Fe^{2+} + S_2O_8^{-}$ (13)

$Fe^{2+} + S_2O_8^{2-} \rightarrow Fe^{3+} + SO_4^{\bullet-}{}_{free} + SO_4^{2-}$ (14)

$SO_4^{\bullet-} / \bullet OH + AO7 \rightarrow CO_2 + H_2O$ (15)

3.4 Stability and reusability of Co-Fc-MOFs

In order to test the stability and reusability of the catalytic performances of Co-Fc-MOFs during continuous operation, it was carried out under the same catalytic conditions. After three cycles, the catalytic performance only slightly decreased from 99.5–90% (Fig. 11), which proved the excellent reusability of Co-Fc-MOFs for PS activation. The non-negligible degradation of catalytic performance may be caused by the adsorption of PS or degradation products covering the surface sites, which would be detrimental to the catalyst (Shu et al. 2020). The decrease in efficiency as the number of cycles increases can be explained by the decrease in the amount of cobalt that has the main catalytic effect in the catalyst in each cycle. After each reaction, the amount of Fe and Co ions leached from Co-Fc-MOFs were detected, and they were found to be lower than 0.1 mg/L in the solution, which contributed little to the degradation of AO7 in the reaction. In addition, the XPS spectra of the fresh and the reacted catalysts were shown in Fig. 9, indicating that the structure of the catalyst did not change during the reaction. In conclusion, the stability and reusability of Co-Fc-MOFs catalyst were satisfactory for the degradation of AO7 in the presence of persulfate.

4. Conclusions

In this study, three heterogeneous catalysts were synthesized by simple chemical methods. The results showed that the Co-Fc-MOFs catalyst can efficiently activate PS to remove AO7. Compared with Fe-Fc-MOFs and Mn-Fc-MOFs, Co-Fc-MOFs shows better catalytic activity and reusability. It can be explained that the presence of cobalt ions successfully improved the removal efficiency of AO7 and promoted the Co^{2+}/Co^{3+} redox cycle. This work provides new ideas for the development and rational design of high-efficiency heterogeneous catalysts.

Declarations

Ethics approval and consent to participate

Not applicable.

Consent for publication

Not applicable.

Availability of data and materials

All data generated or analysed during this study are included in this published article.

Competing interests

The authors declare that they have no competing interests.

Funding

This work was financially supported by the National Natural Science Foundation of China (Grant Nos. 41877132, 51578264 and 51908242).

Authors' contributions

XL analyzed and interpreted the data and was a major contributor in writing the manuscript. XR performed formal analysis, writing-review & editing and supervision. YL performed investigation and formal analysis. RW performed Visualization, Supervision. YW performed validation and formal analysis. WG performed supervision, conceptualization, resources, writing-reviewing and editing, project administration and funding acquisition. All authors read and approved the final manuscript.

Acknowledgements

This work was financially supported by the National Natural Science Foundation of China (Grant Nos. 41877132, 51578264 and 51908242).

References

Ahmadi M, Ghanbari F, Alvarez A, Martinez SS (2017) UV-LEDs assisted peroxymonosulfate/Fe2+ for oxidative removal of carmoisine: The effect of chloride ion. Kor J Chem Eng 34: 2154-2161. http://doi.org/10.1007/s11814-017-0122-1

Chang JF, Wang X, Wang J, Li HY, and Li F (2019) Nucleic Acid-Functionalized Metal-Organic Framework-Based Homogeneous Electrochemical Biosensor for Simultaneous Detection of Multiple Tumor Biomarkers. Anal Chem 91: 3604-3610. http://doi.org/10.1021/acs.analchem.8b05599

Devic T, Serre C, Audebrand N, Marrot J, Férey G (2005) MIL-103, A 3-D Lanthanide-Based Metal Organic Framework with Large One-Dimensional Tunnels and A High Surface Area. J Ame Chem Soc 127: 12788-12789. http://doi.org/10.1021/ja053992n

Duan PJ, Ma TF, Yue Y, Li YW, Zhang X, Shang YN, Gao BY, Zhang QZ, Yue QY, Xu X (2019) Fe/Mn nanoparticles encapsulated in nitrogen-doped carbon nanotubes as a peroxymonosulfate activator for acetamiprid degradation. Environ Sci Nano 6: 1799-1811. http://doi.org/10.1039/c9en00220k

Eddaoudi M, Kim J, Rosi N, Vodak D, Wachter J, O'keeffe M, Yaghi OM (2002) Systematic design of pore size and functionality in isoreticular MOFs and their application in methane storage. Sci 295: 469-472. http://doi.org/10.1126/science.1067208

Erdem H, Erdem M. (2020) Synthesis and characterization of a novel activated carbon–supported cobalt catalyst from biomass mixture for tetracycline degradation via persulfate activation. Biomass Convers Biorefin. http://doi.org/10.1007/s13399-020-00963-z

Gao YW, Li SM, Li YX, Yao LY, Zhang H (2017) Accelerated photocatalytic degradation of organic pollutant over metal-organic framework MIL-53(Fe) under visible LED light mediated by persulfate. Appl Catal B 202: 165-174. http://doi.org/10.1016/j.apcatb.2016.09.005

Ghanbari F, Moradi M (2017) Application of peroxymonosulfate and its activation methods for degradation of environmental organic pollutants: Review. Chem Eng J 310: 41-62. http://doi.org/10.1016/j.cej.2016.10.064

He CB, Lu KD, Liu DM, Lin WB (2014) Nanoscale metal-organic frameworks for the co-delivery of cisplatin and pooled siRNAs to enhance therapeutic efficacy in drug-resistant ovarian cancer cells. J Am Chem Soc 136: 5181-5184. http://doi.org/10.1021/ja4098862

Huo J, Wang L, Irran E, Yu HJ, Gao JM, Fan DS, Li B, Wang JJ, Ding WB, Amin AM, Li C, Ma L (2010) Hollow ferrocenyl coordination polymer microspheres with micropores in shells prepared by Ostwald ripening. Angew Chem Int Ed Engl 49: 9237-9241. http://doi.org/10.1002/anie.201004745

Huo J, Wang L, Irran E, Yu HJ, Ma L, Gao JM, Fan DS, Ding WB, Amin AM, Tai YL (2012) Synthesis, characterization and magnetic properties of hollow microspheres with micro-mesoporous shells assembled from cobalt-based ferrocenyl coordination polymers. J Colloid Interface Sci 367: 92-100. http://doi.org/10.1016/j.jcis.2011.07.099

Khatri A, Peerzada MH, Mohsin M, White M (2015) A review on developments in dyeing cotton fabrics with reactive dyes for reducing effluent pollution. J Cleaner Prod 87: 50-57. http://doi.org/10.1016/j.jclepro.2014.09.017

Li HX, Xu SD, Du J, Tang JH, Zhou QW (2019) Cu@Co-MOFs as a novel catalyst of peroxymonosulfate for the efficient removal of methylene blue. RSC Adv 9: 9410-9420. http://doi.org/10.1039/c9ra01143a

Li RC, Jin XY, Megharaj M, Naidu R, Chen ZL (2015) Heterogeneous Fenton oxidation of 2,4-dichlorophenol using iron-based nanoparticles and persulfate system. Chem Eng J 264: 587-594. http://doi.org/10.1016/j.cej.2014.11.128

Li YW, Yang RT (2007) Gas adsorption and storage in metal-organic framework MOF-177. Langmuir 23: 12937-12944. http://doi.org/ 10.1021/la702466d

Liang CJ, Su HW (2009) Identification of Sulfate and Hydroxyl Radicals in Thermally Activated Persulfate. Ind Eng Chem Fundam 48: 472-475. http://doi.org/10.1021/ie9002848

Liu YL, Eubank JF, Cairns AJ, Eckert J, Kravtsov VC, Luebke R, Eddaoudi M (2007) Assembly of Metal–Organic Frameworks (MOFs) Based on Indium-Trimer Building Blocks: A Porous MOF with soc Topology and High Hydrogen Storage. Angew Chem Int Ed 119: 3342-3347. http://doi.org/10.1002/ange.200604306

Liu ZQ, Cheng H, Li N, T. Ma TY, Su YZ (2016) ZnCo2O4 Quantum Dots Anchored on Nitrogen-Doped Carbon Nanotubes as Reversible Oxygen Reduction/Evolution Electrocatalysts. Adv Mater 28: 3777-3784. http://doi.org/10.1002/adma.201506197

Liu Z, Su RD, Sun X, Zhou WZ, Gao BY, Yue QY, Li Q (2020) The obvious advantage of amino-functionalized metal-organic frameworks: As a persulfate activator for bisphenol F degradation. Sci Total Environ. 741: 140464. http://doi.org/10.1016/j.scitotenv.2020.140464

Marija M, Marinović S, Mudrinić T, Ajduković M, Jović-Jovičić N, Mojović Z, Orlić J, Milutinović-Nikolić A, Banković P (2019) Co(II) impregnated Al(III)-pillared montmorillonite–Synthesis, characterization and catalytic properties in Oxone® activation for dye degradation. Applied Clay Science 182: 105276. http://doi.org/10.1016/j.clay.2019.105276

Mu BN, Liu LY, Li W, Yang YQ (2019) A water/cottonseed oil bath with controllable dye sorption for high dyeing quality and minimum discharges. J Cleaner Prod 236: 117566. http://doi.org/10.1016/j.jclepro.2019.07.041

Shu YR, Zhang P, Zhong YJ, Xu XY, Ren GK, Wang W, Xiang HL, Zhang ZY, Yang XY, Wang XL (2020) Heterogeneous activation of persulfate by ZnCoxFe2−xO4 loaded on rice hull carbon for degrading bisphenol A. RSC Adv 10: 44551-44570. http://doi.org/10.1039/d0ra08852h

Stroever S, Hayes K, Hice JL, Baldauf G, Woodard C, Martin R (2015) Construction and Implementation of an Operating Room Management Plan for the Prevention of Perioperative Hypothermia. Am J Infect Control 43: S12-S13. http://doi.org/10.1016/j.ajic.2015.04.031

Su SN, Guo WL, Leng YQ, Yi CL, Ma ZM (2013) Heterogeneous activation of Oxone by CoxFe3-xO4 nanocatalysts for degradation of rhodamine B. J Hazard Mater 244-245: 736-742. http://doi.org/10.1016/j.jhazmat.2012.11.005

Usman M, Faure P, Ruby C, Hanna K (2012) Application of magnetite-activated persulfate oxidation for the degradation of PAHs in contaminated soils. Chemosphere 87: 234-240. http://doi.org/10.1016/j.chemosphere.2012.01.001

Wacławek S, Lutze HV, Grübel K, Padil VVT, Černík M, Dionysiou DD (2017) Chemistry of persulfates in water and wastewater treatment: A review. Chem Eng J 330: 44-62. http://doi.org/10.1016/j.cej.2017.07.132

Xiong CY, Wang HJ, Liang WB, Yuan YL, Yuan R, Chai YQ (2015) Luminescence-Functionalized Metal-Organic Frameworks Based on a Ruthenium(II) Complex: A Signal Amplification Strategy for Electrogenerated Chemiluminescence Immunosensors. Chemistry 21: 9825-9832. http://doi.org/10.1002/chem.201500909

Yang X, Lv JJ, Yang ZH, Yuan R, Chai YQ (2017) A Sensitive Electrochemical Aptasensor for Thrombin Detection Based on Electroactive Co-Based Metal-Organic Frameworks with Target-Triggering NESA Strategy. Anal Chem 89: 11636-11640. http://doi.org/10.1021/acs.analchem.7b03056

Figures

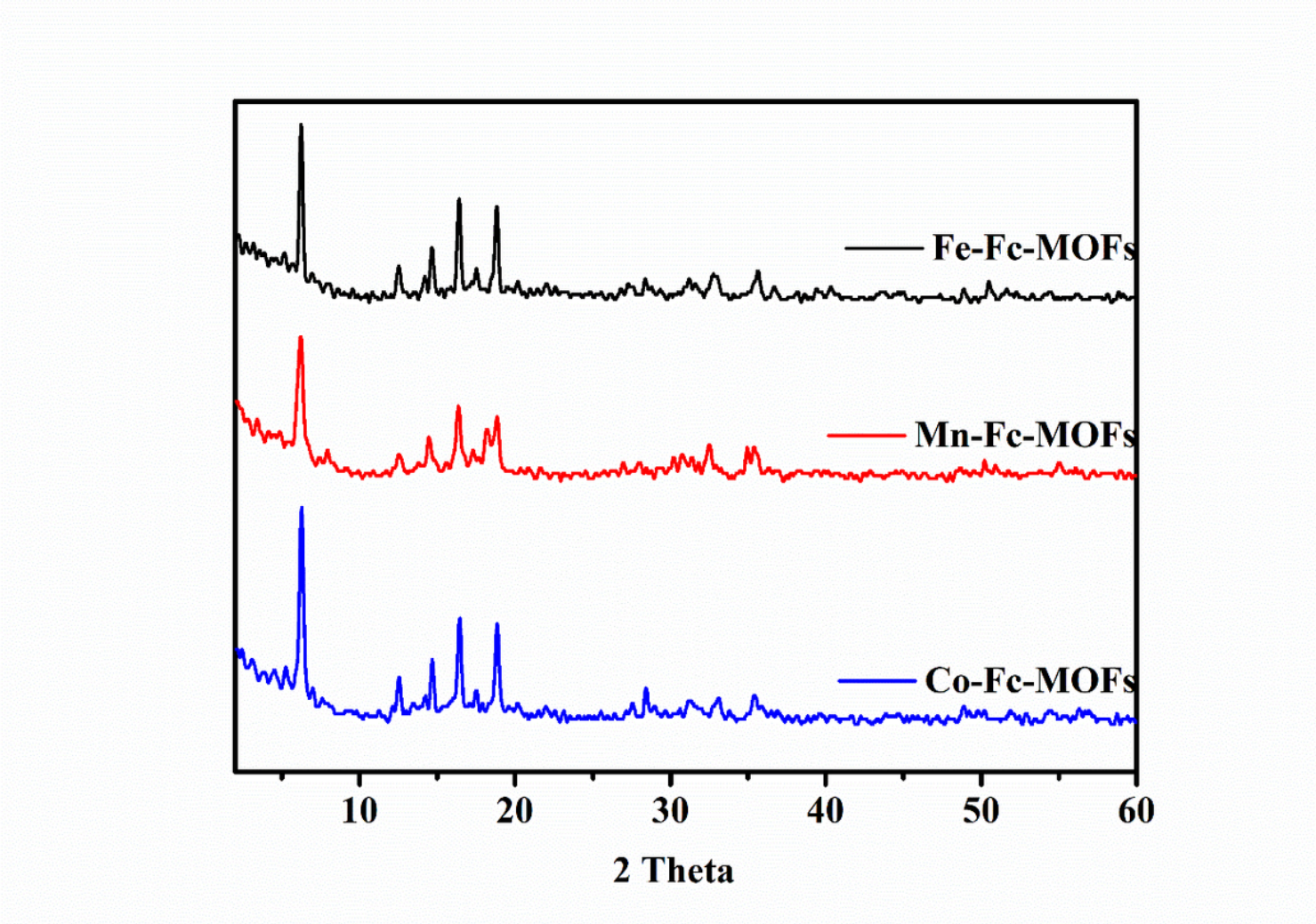

Figure 1

XRD patterns of Fe-Fc-MOFs, Mn-Fc-MOFs and Co-Fc-MOFs.

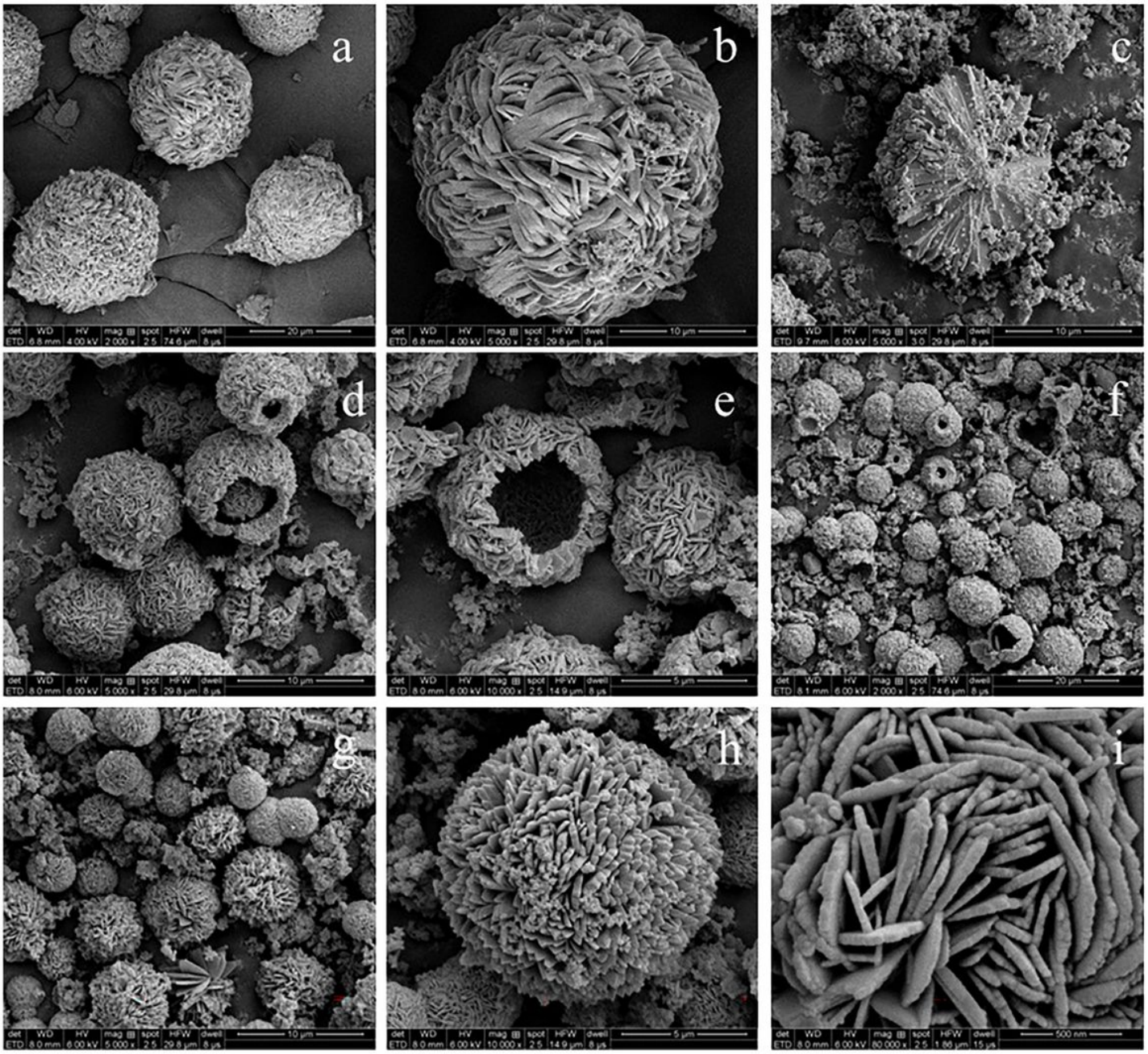

Figure 2

SEM images of Fe-Fc-MOFs (a, b and c), Mn-Fc-MOFs (d, e and f) and Co-Fc-MOFs (g, h and i).

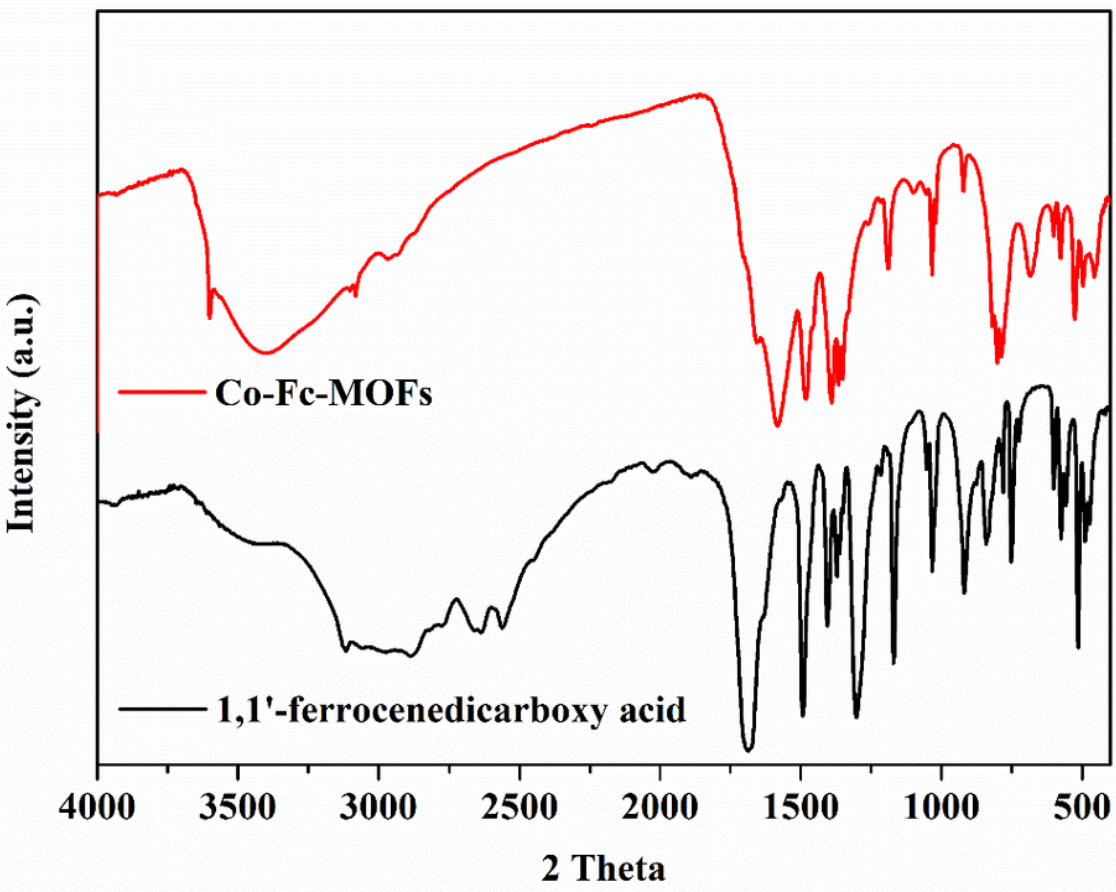

Figure 3

FTIR spectra of Co-Fc-MOFs and 1, 1’-ferrocenedicarbpxy acid.

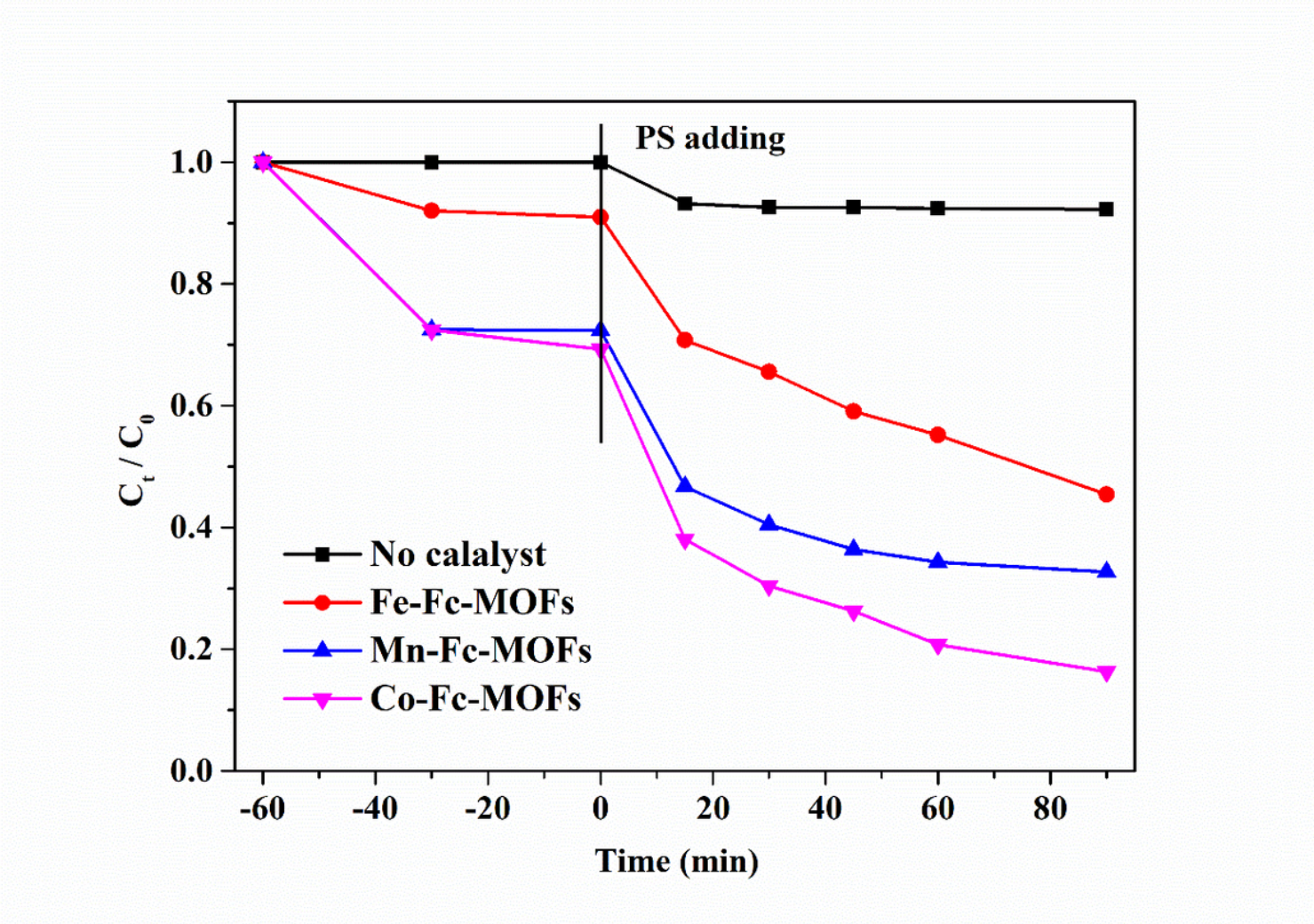

Figure 4

Removal of AO7 with different reaction conditions ([AO7] = 20 mg/L, [catalyst] = 0.25 g/L, [persulfate] = 4 mmol/L, pH = 7.01).

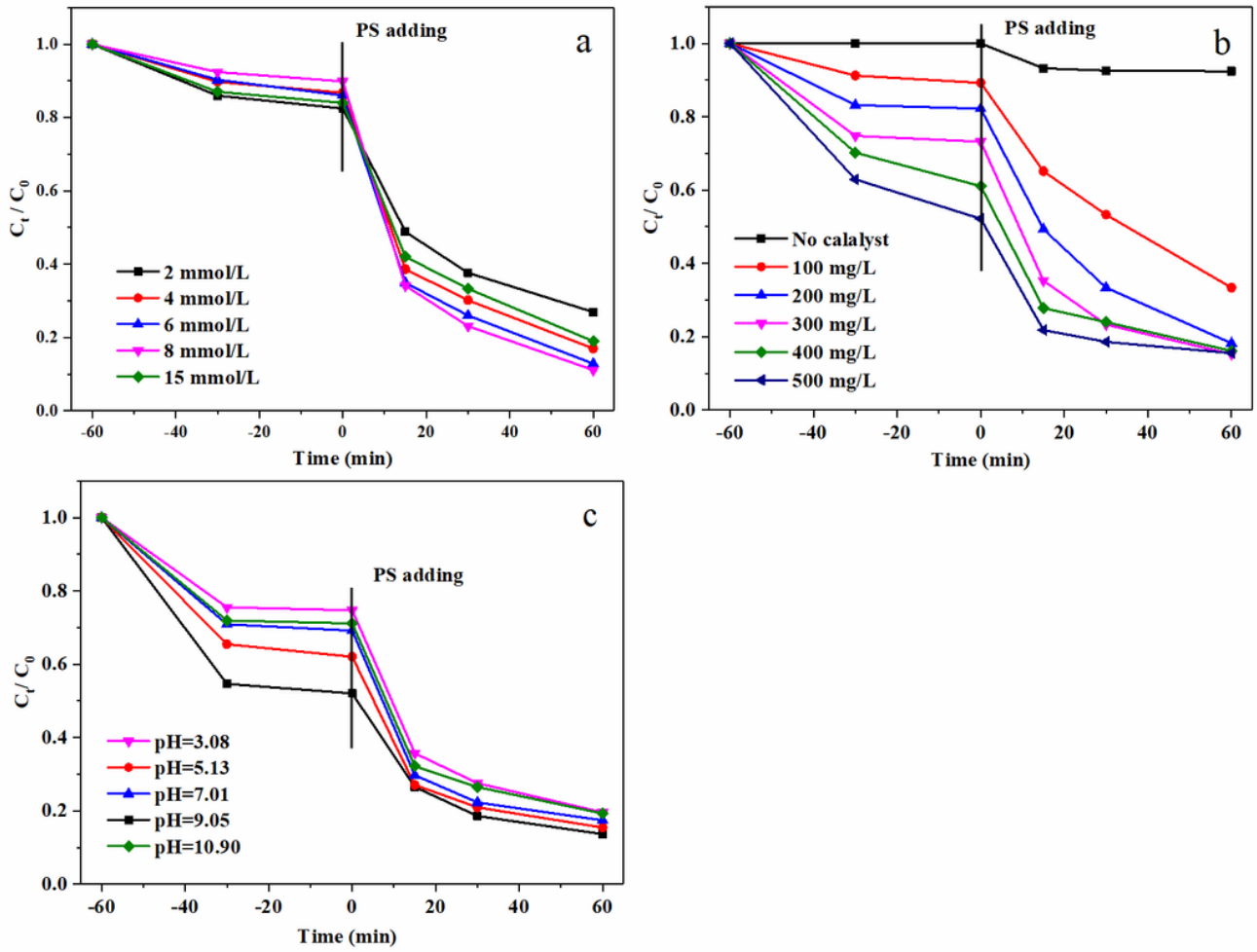

Figure 5

Effects of (a) persulfate concentration, (b) Co-Fc-MOFs dosage, (c) initial pH on the degradation of AO7.

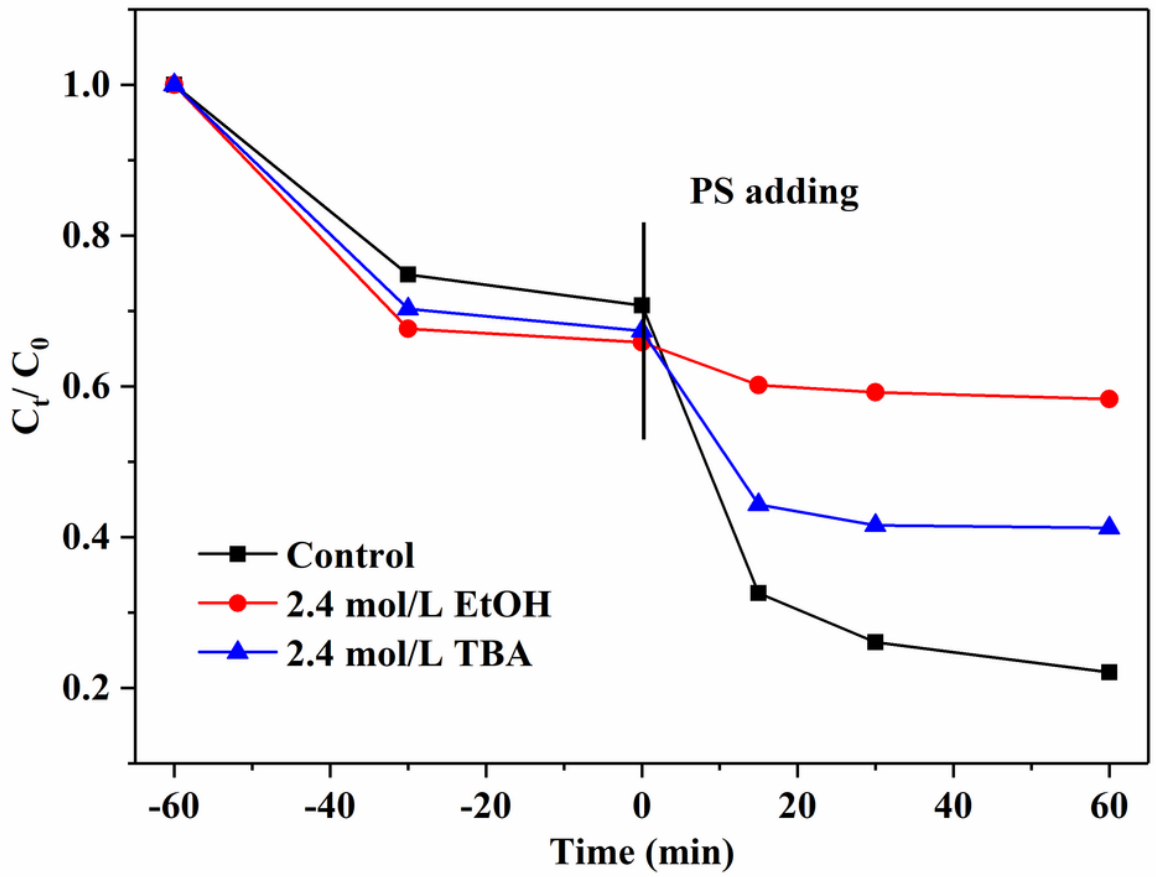

Figure 6

Effects of EtOH and TBA on the removal of AO7.

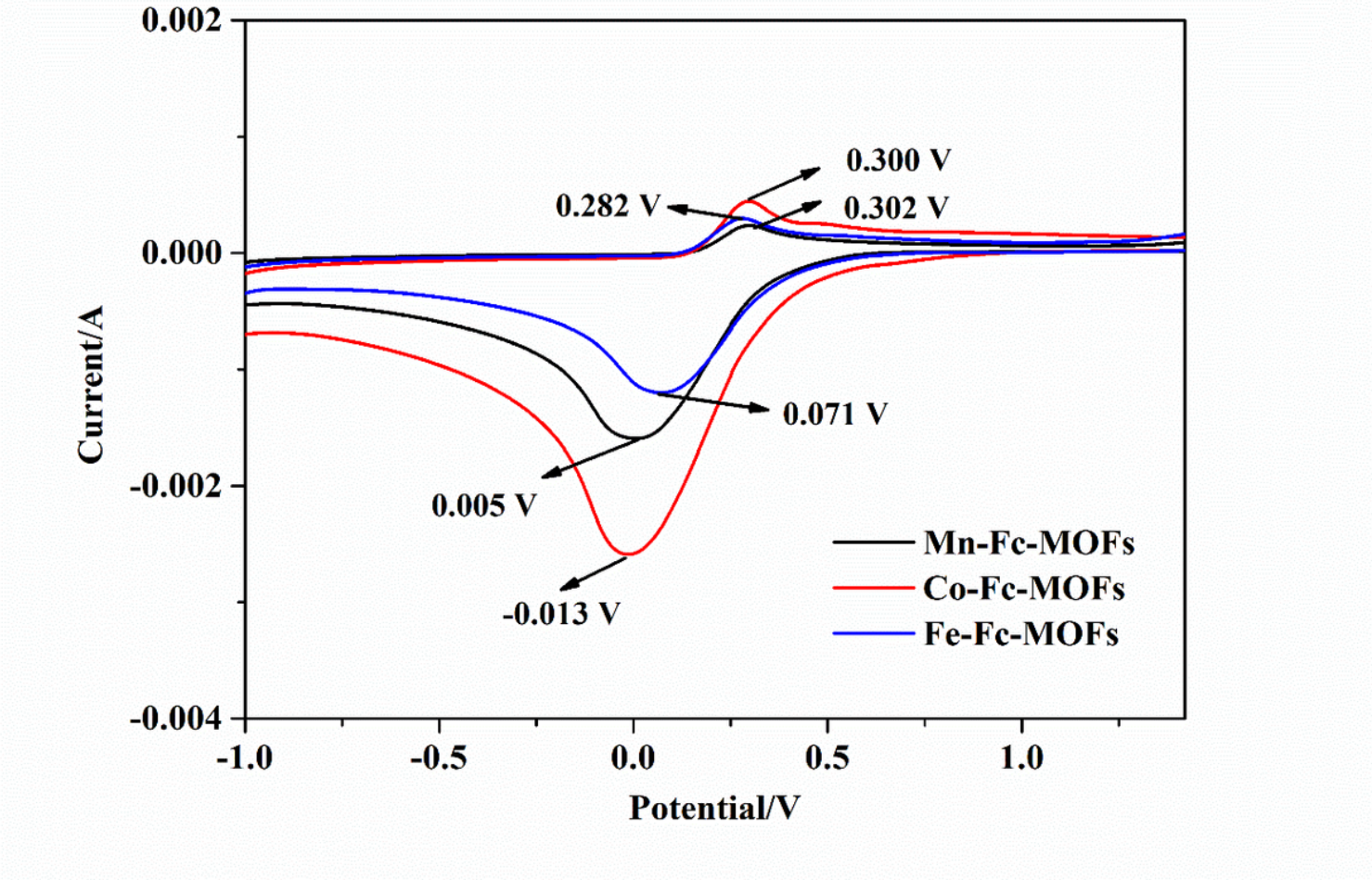

Figure 7

Cyclic voltametric (CV) of Fe-Fc-MOFs, Mn-Fc-MOFs and Co-Fc-MOFs.

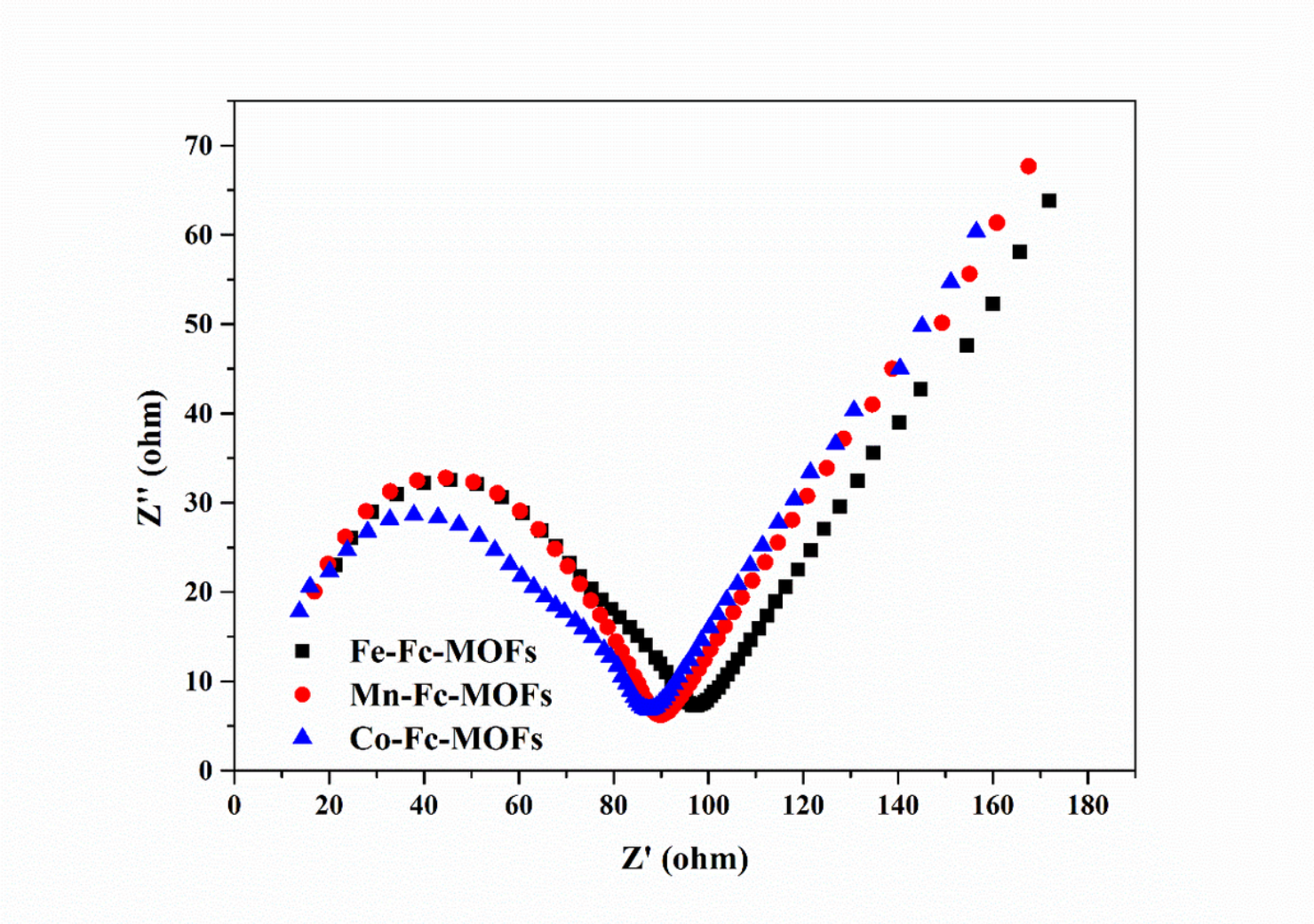

Figure 8

EIS Nyquist plots of Fe-Fc-MOFs, Mn-Fc-MOFs and Co-Fc-MOFs electrodes.

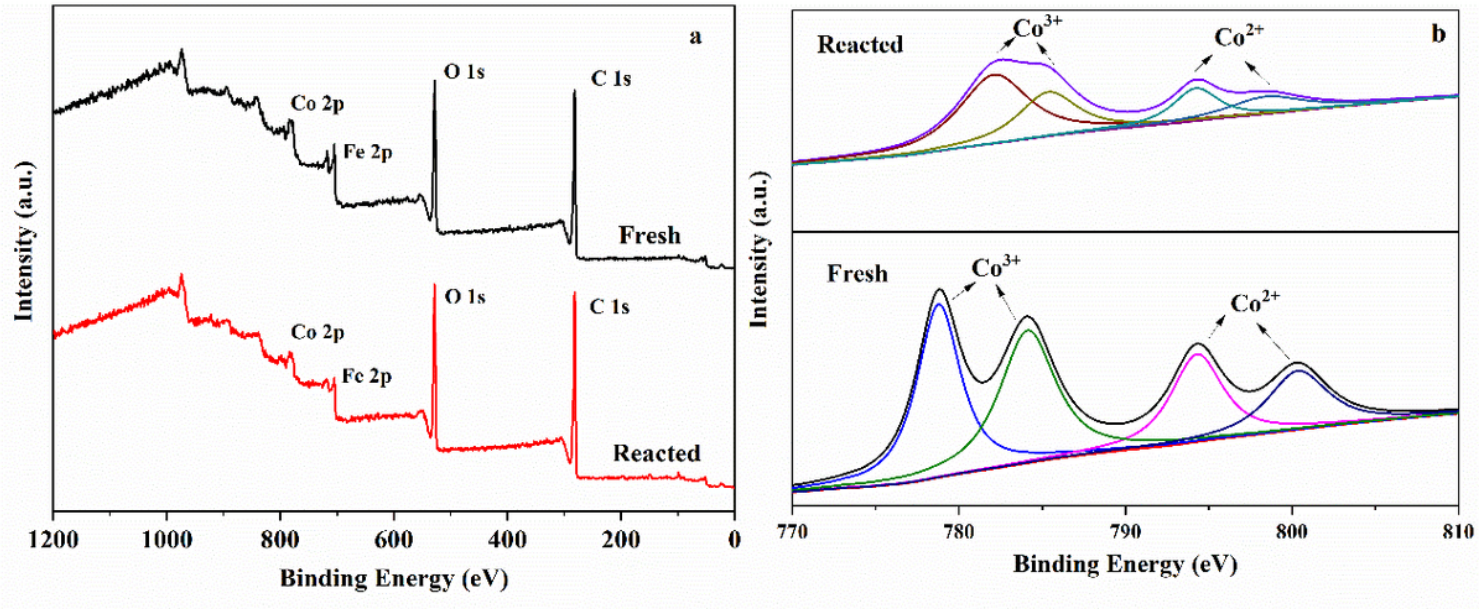

Figure 9

XPS spectra of Co-Fc-MOFs before and after use, (a) full-range scan of the samples and (b) Co 2p.

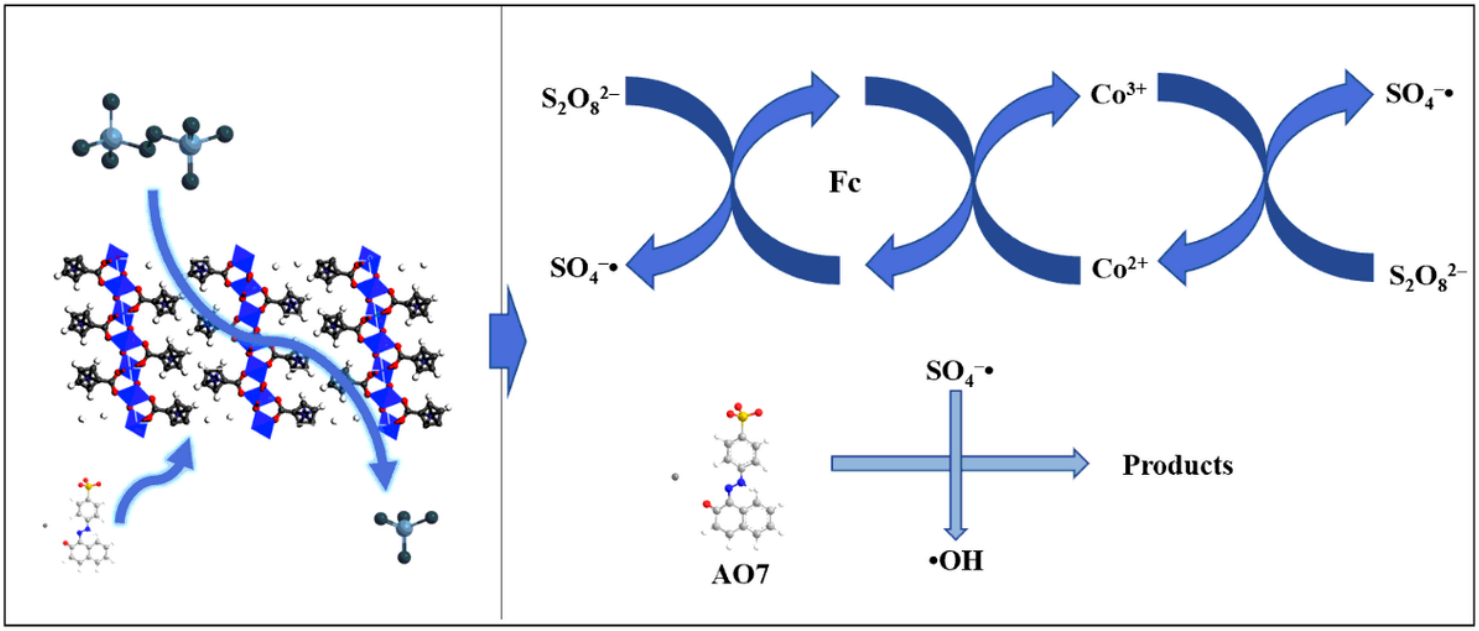

Figure 10

A schematic illustration of catalytic oxidation of AO7 over Co-Fc-MOFs.

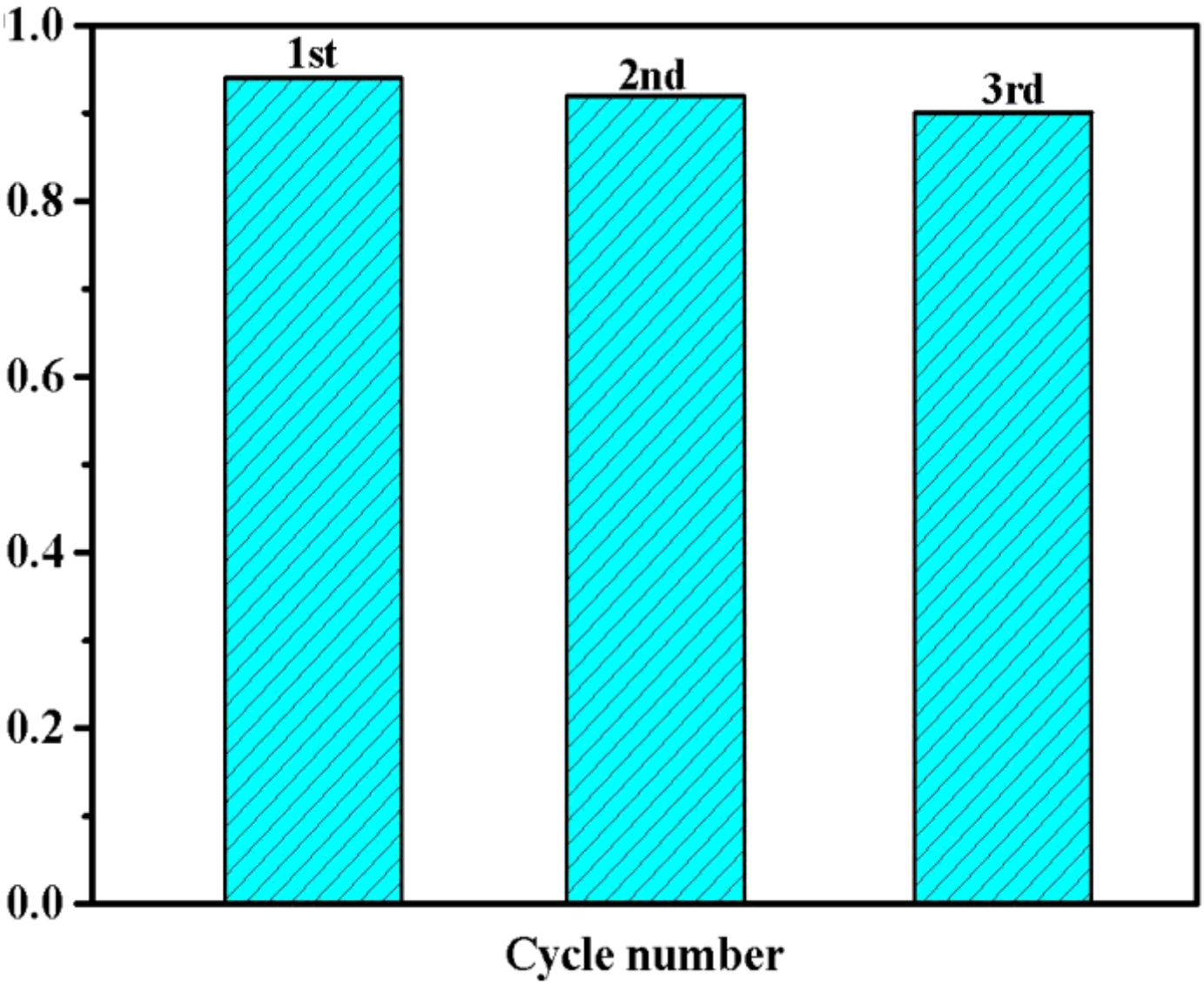

Figure 11

AO7 removal efficiencies of recycled Co -Fc-MOFs.